



Semi-automatic Integration of Panoramic Hyperspectral Imagery with Photorealistic Lidar Models

ALEKSANDRA SIMA, SIMON J. BUCKLEY, TOBIAS H. KURZ, Bergen, Norway & DANILO SCHNEIDER, Dresden

Keywords: registration, hyperspectral, TLS, lidar, photorealistic models

Summary: This paper presents a method for increasing the automation of the registration of panoramic hyperspectral images with co-registered conventional digital imagery and a point cloud acquired with a terrestrial laser scanner (lidar), for geological purposes. The SIFT (scale invariant feature transform) interest operator is used to find homologous points between the two imagery types which, because they are recorded at different spectral ranges (visible and short wave infrared) using different geometric projections, differ significantly in appearance. After reducing false matches using RANSAC (random sample consensus), a geometric model for panoramic cameras is applied to retrieve the orientation parameters of the hyperspectral scenes. Once registered, hyperspectral classifications can be combined with the lidar geometry in photorealistic models, allowing material information to be linked to object geometry. Improved automation of the data registration reduces processing time and makes the domain more accessible for non-specialists.

Zusammenfassung: *Semi-automatische Integration von hyperspektralen Panoramabildern mit fotorealistischen Lidar-Modellen.* Mit diesem Beitrag wird eine Methode zur semi-automatischen Registrierung von hyperspektralen Panoramabildern mit konventionellen digitalen Fotos sowie mit den Punktwolken eines terrestrischen Laserscanners (Lidar) beschrieben. Die Methode wird für geologische Fragestellungen angewendet. Es wird gezeigt, dass der SIFT (Scale Invariant Feature Transform) Operator zur automatischen Auffindung homologer Punkte in den verschiedenen Bilddaten trotz der verschiedenen Spektralbereiche (sichtbarer sowie infraroter Bereich) und unterschiedlicher Bildgeometrien (zentralperspektivische Bilder und Panoramabilder mit zylindrischer Projektion) verwendet werden kann. Falsch positive Punkte werden mit der RANSAC (Random Sample Consensus) Methode ausgeschlossen. Unter Anwendung eines Panoramakameramodells können anschließend die äußere und innere Orientierung der hyperspektralen Bilder ermittelt werden. Mit Kenntnis der inneren und äußeren Orientierung können dann einerseits die vermaschten Lidar-Modelle fotorealistisch texturiert und andererseits mit hyperspektralen Klassifikationen geometrisch korrekt überlagert werden, womit eine Verlinkung von geometrischen mit geochemischen Informationen ermöglicht wird. Eine verbesserte Automatisierung der Datenregistrierung verkürzt die Bearbeitungszeit und erleichtert die Datenintegration für fachfremde Anwender.

1 Introduction

The technique of hyperspectral imaging has been used for many years, mostly applied from airborne or satellite-borne platforms. Recent technological advances have given rise to ter-

restrial hyperspectral imaging sensors, and these are being applied in an increasingly diverse range of laboratory and field settings, including surgery, food safety, surveillance and geology. These hyperspectral sensors record the light reflected from an object in hundreds

of narrow (3–15 nm) spectral bands, allowing creation of near-continuous spectral curves that can be used for the analysis of absorption properties (VAN DER MEER 2004), detection of subtle geochemical differences (CLARK et al. 1990) or quantitative analysis of pixel composition (CLARK & ROUSH 1984). Hyperspectral imaging is an established method, allowing different materials to be mapped and quantified, even where differences are indistinguishable with the naked eye.

Photorealistic 3D models created from terrestrial laser scanners (TLS, also known as lidar) and digital semi-metric imagery have been widely used in geological applications (BELLIAN et al. 2005, BUCKLEY et al. 2008), and geomatics techniques are becoming prevalent in the field of outcrop geology. Geological outcrops are exposed cliff sections or quarries that, when captured in 3D, can help to improve the understanding of geometrical relationships between geological features. High-accuracy and high-resolution 3D models of geological outcrops are used to extract statistical data, such as sizes of features, thicknesses of strata, or surface orientation, as well as for interpretation and educational purposes (BELLIAN et al. 2005, BUCKLEY et al. 2008, 2010). However, mineralogical and lithological mapping is normally limited to interpretation of the three standard spectral bands (red, green, blue; RGB) acquired in the visible spectrum by the conventional digital camera. Many minerals exist that cannot be distinguished using visible light, but that exhibit specific absorption and reflectance properties in the infrared region of the electromagnetic spectrum (e.g. limestone and dolomite; CLARK et al. 1990). Therefore, complementing the photorealistic 3D outcrop models with auxiliary spectral data, in the form of hyperspectral imagery, can provide domain experts with additional geochemical information, adding great potential to studies of mineralogy and lithology (KURZ et al. 2012). This goal relies on the accurate registration of the component data types.

In this paper the first results are presented of a semi-automatic method for registration of terrestrial panoramic hyperspectral imagery with data acquired by a laser scanner with an integrated standard digital camera.

The resulting orientation parameters of the hyperspectral images establish their position and orientation relative to the point cloud and enable enhancement of the photorealistic outcrop models with classification products. The required processing steps are implemented as a series of Matlab (MathWorks) scripts. As such, automated image registration methods are highly desired to reduce processing time, improve registration accuracy, and make the method more accessible for non-specialists. The data used in this project were acquired for the purposes of geological studies, though the workflow is application-independent, and can be applied analogously in other disciplines.

2 Background

Although lidar systems primarily record geometric data, in the form of the point cloud, many systems record ancillary information pertaining to the strength of the returned laser signal, known as intensity or amplitude. Lidar intensity data can be used to register auxiliary image data in the scanner coordinate system. FURUKO & KING (2004) registered conventional photos using tie points between the photos and synthetic images created from the point cloud intensity values. BÖHM & BECKER (2007) and GONZALEZ-AGUILERA et al. (2009) registered multiple scan positions on the basis of control points matched between digital photos and the intensity images recorded by a TLS. The success of using lidar intensity for registration purposes is reliant on the signal digitization depth (dynamic range) being of sufficient quality to identify strong features for determining correspondence.

Several successful attempts have been made to integrate terrestrial hyperspectral data with lidar and image data. KURZ et al. (2011) automatically measured reflective targets and manually selected additional natural tie points between the point cloud and hyperspectral image in order to ensure a uniform point distribution. Exterior image orientations and intrinsic panoramic hyperspectral camera parameters were determined in a bundle block adjustment. The authors reported difficulties with the manual, and time-consuming, measurement of tie points between the point

cloud and the spectral image, and they instead manually located homologous points between a textured photorealistic model and the hyperspectral images. NIETO et al. (2010) developed a framework aiming to obtain a detailed 3D geological map of the environment in an automated manner, using TLS, visible spectrum photography and very near infrared spectral imagery. Piecewise linear transformation was used to register the hyperspectral data, based on natural features found by the scale invariant feature transform (SIFT; LOWE 1999) interest operator between a 2D image formed from the coloured (RGB) point cloud and the true colour image composition created from the hyperspectral data.

In contrast to the work presented in NIETO et al. (2010), the hyperspectral imagery used in the current study does not cover the visible light spectrum, and therefore automated measures must handle the significantly different grayscale values between the conventional photographs and the short wave infrared (SWIR) imagery (Fig. 1).

The SIFT operator (LOWE 1999) is one of the most frequently used interest operators, and is employed in computer vision for many different purposes, such as 3D matching, 3D scene reconstruction, panorama stitching and motion tracking. The advantage of SIFT over other interest operators traditionally used in photogrammetry, such as the Förstner operator (FÖRSTNER 1986) or Harris operator (HARRIS & STEPHENS 1988), is the capability to deliver reliable results under difficult geometric and radiometric conditions (JAZAYERI & FRASER 2010, OSTIAK 2006). These proper-

ties were important in this study, where homologous (corresponding) points needed to be found between images acquired in varying parts of the electromagnetic spectrum (Fig. 1). The behaviour and efficiency of the SIFT interest operator has been mostly documented when applied to images of man-made features with many edges, corners and relatively regular patterns (PICARD et al. 2009). In contrast, geological outcrops have a completely different scene composition and character, with natural features, few hard edges and irregular texture (Fig. 1). Additionally, the two image types to be matched in this study are acquired using different projections (central perspective and cylindrical panoramic) and with different resolutions. Such environments can be challenging for interest operators, especially if the distribution of identified points, used as tie points in later stages of processing, is of high importance.

3 Data Characteristics

The datasets used in this study were acquired in two different locations, in Spain and Norway. Data collection in the Pozalagua quarry in Cantabria, northern Spain, had the geological aim to map the distribution of sedimentary products such as limestone, different types of dolomite and calcite (KURZ et al. 2012). The main objective of the data collection in the second location, the GUSDAL quarry near Åheim in central-West Norway, was to map the degree of serpentinization in ultramafic rocks. Because the rock types in the two



Fig. 1: Detail of a Nikon D200 photo; left: RGB; middle: greyscale; right: the corresponding part of a HySpex image, 1.629 μm wavelength.

quarries were different, their appearance in the images varies, creating different environments for tie point extraction.

Data were acquired with two separate systems, a portable hyperspectral HySpex SWIR-320m camera (Norsk Elektro Optikk AS), and a Riegl LMS-Z420i (RIEGL 2012) terrestrial laser scanner with a Nikon D200 camera mounted on top. Both systems were located close to each other (very short baseline, c. 1.5 m) at the time of data acquisition in order to reduce differences in the viewing angle of the sensors. The exposure position of the HySpex sensor was included in an overview lidar scan so that the relative position of the two instruments was recorded.

3.1 Hyperspectral Imagery

The HySpex SWIR-320m is a portable terrestrial hyperspectral line scanner, with a 14° field of view across track. The sensor covers the spectral range from 1.3 μm to 2.5 μm over 241 bands, with a sampling interval of 5 nm and has 320 pixels in the across track direction. As a pushbroom linear-array sensor, the system uses a rotation stage to construct the image in the along-track direction. This results in cylindrical imaging geometry, which must be modelled to allow a precise coupling with the lidar and conventional image data. The sensor can be successfully represented by a geometric model for panoramic cameras (SCHNEIDER & MAAS 2006), as described in (KURZ et al. 2011).

From the Pozalagua quarry two hyperspectral scans were used, of size 320 pixels x 1200 pixels (image B1) and 320 pixels x 1500 pixels (B2), and with a ground pixel size varying between 0.06 m and 0.09 m at ranges between 60 m and 130 m. From the dataset acquired at Gusdal quarry, one hyperspectral scan was used (A1), of size 320 pixels x 1000 pixels. With a scanning range of c. 20 m, this resulted in a ground sample distance of c. 0.015 m. Imagery was collected to maximize coverage of the geology in the limited field time, rather than for the photogrammetric configuration (KURZ et al. 2011).

3.2 Digital Photos

A 10.2 megapixel Nikon D200 single-lens reflex (SLR) camera was mounted on top of the terrestrial laser scanner. Two different lenses were used while acquiring data for this study: a Nikkor 85 mm lens (Pozalagua quarry), and a Nikkor 50 mm lens (Gusdal quarry). The interior orientation of the lenses was calibrated and the focal lengths fixed for the duration of the data collection. The position of the camera was calibrated relative to the scanner centre, so that the photographs could be easily registered in the lidar coordinate system and further used for texturing of the lidar surface model (BUCKLEY et al. 2010).

The difference in optical construction and much higher sensor resolution of the Nikon camera resulted in a significantly better ground sampling distance when compared to the hyperspectral images, being between 0.004 m and 0.009 m for the Spain dataset and around 0.003 m in the Gusdal quarry. Horizontal and vertical fields of view of the Nikon D200 camera are 10.6° and 15.8° for the 85 mm lens and 18.0° and 26.6° for the 50 mm lens. The photos were collected with a 10% horizontal overlap, so that several photos are often necessary to cover the area of one HySpex image or lidar scan (see example in Fig. 4).

3.3 Lidar Point Cloud

The Riegl LMS-Z420i is a long range, high performance terrestrial scanner capable of delivering points with accuracy (1σ) of 0.01 m and average repeatability of 0.004 m at the range of 50 m (RIEGL 2012). The scan distance at the Pozalagua quarry varied between 60 m and 130 m, and the resulting point density was 0.05 m to 0.10 m. At the Gusdal quarry the scanner was located at a distance of 20 m from the outcrop wall, resulting in a point cloud density of around 0.03 m. The collected point clouds and digital imagery were processed as in BUCKLEY et al. (2010) to obtain a photorealistic model for each site.

4 Data Integration Workflow

In order to integrate hyperspectral imagery into the lidar coordinate system, 3D control points need to be determined between the hyperspectral panoramic images and the data collected by the TLS system. Because the dynamic range of the point cloud intensity values recorded by the LMS-Z420i scanner was very low, it was not possible to create a synthetic intensity image with quality high enough for interest point extraction. Instead, the registered Nikon photos were used as the reference dataset, and hyperspectral panoramas were matched with these. The SIFT interest operator was used to find natural tie points between the hyperspectral imagery and the photos acquired by the Nikon camera (orange block in Fig. 2). Because of significant disparities between these two datasets, the interest operator algorithm was configured to yield as many points as possible, though a high number of false matches resulted. Therefore, robust homography model fitting using random sample consensus method (RANSAC) (FISCHLER & BOLLES 1981) was applied in order to ensure the correct linking of conjugate points. 3D object coordinates of the matched points were obtained by subpixel interpolation within the point cloud backprojected on the image plane (blue block in Fig. 2). Finally, exterior orientation parameters of the hyperspectral image were established by spatial resection using the

identified point pairs and the geometric model for panoramic cameras described in SCHNEIDER & MAAS (2006) (green block in Fig. 2).

4.1 Preprocessing of the Hyperspectral Imagery

Firstly, raw spectral data acquired by the HySpex SWIR-320m sensor were converted into at-sensor radiances, according to the spectral calibration report provided by the sensor manufacturer. Each hyperspectral image consists of 241 very narrow spectral bands. Some of these bands contain only random noise, as certain wavelengths are completely absorbed by the atmosphere, and others are highly correlated with neighbouring bands. Many different methods exist to reduce the dimensionality of the data, and most of these are based on principal component analysis (PCA), relying on several preprocessing steps (de-striping, bad pixel interpolation, correction of brightness gradients). All these corrections are crucial for the final spectral mapping procedures but they also change locally the digital number values of the image. The influence of this change depends strongly also on the correction algorithm applied. In order to make the hyperspectral image registration independent of the spectral processing workflow, it was decided to make use of the almost unchanged at-sensor radiance images.

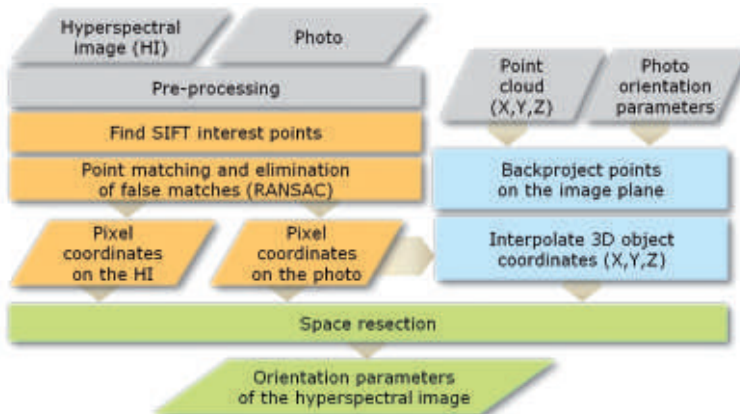


Fig. 2: General processing workflow.

4.2 Preprocessing of the Photos

Because the SIFT interest operator is applied to a single image band, the conventional photos (RGB) needed to be transformed into a single-band greyscale image. This conversion was performed according to the national television systems committee (NTSC) standard conversion (DURDA 2012) used for calculating the effective luminance of a pixel.

Even though the interest point operator used in this study is robust to small projection differences (LINGUA et al. 2009, LOURENCO et al. 2012), in order to guarantee optimized conditions for the automatic tie point selection procedure, photos were reprojected from the central perspective projection to the (hyperspectral) cylindrical panoramic projection taking into account interior orientation parameters and lens distortion. Furthermore, in order to optimize images for the matching purposes and shorten the processing time, the Nikon photos were downsampled by a scale factor approximately equal to the ratio of the differences in pixel dimensions between the two data types. Special attention must be paid when selecting the downsampling algorithm, as the entire resampling process must be traceable so that the photo interior orientation parameters from the downsampled image can be restored. The result of this stage is that both hyperspectral and standard photos are in the same geometric projection, and have near-identical ground sample distances.

4.3 SIFT Interest Points and Image Matching

Hyperspectral images consist of hundreds of spectral bands, but, as previously mentioned, the SIFT detector operates only on a single image band. An attempt to merge all the points correctly matched between all the hyperspectral image bands and the Nikon photos revealed a small band mis-registration in the HySpex SWIR-320m sensor, most likely caused by a keystone effect (NEVILLE et al. 2004). It was therefore decided to identify one spectral band that was optimal for matching with the overlapping Nikon photos. The criterion used in this selection procedure was the maximum total number of points matched between the spectral band and all the overlapping Nikon images. In the cases where several spectral bands had an equal total number of control points found, priority was given to the band with the highest minimum number of points matched for a single photo.

Using the described selection procedure, bands 61 (1.629 μm) and 78 (1.712 μm) were selected respectively as the best wavelengths for tie point extraction purposes for the Pozalagua B1 and B2 hyperspectral images (Fig. 3). In the dataset from the Gusal quarry the 2.326 μm wavelength (band 204) was chosen. The troughs in Fig. 3 where very few points were matched correspond to spectral bands strongly affected by atmospheric absorption.

The VLFeat open source library (VEDALDI & FULKERSON 2008), containing implementations of the SIFT detector and descriptor, together with a matching procedure, was used for the purposes of this study. In order to yield

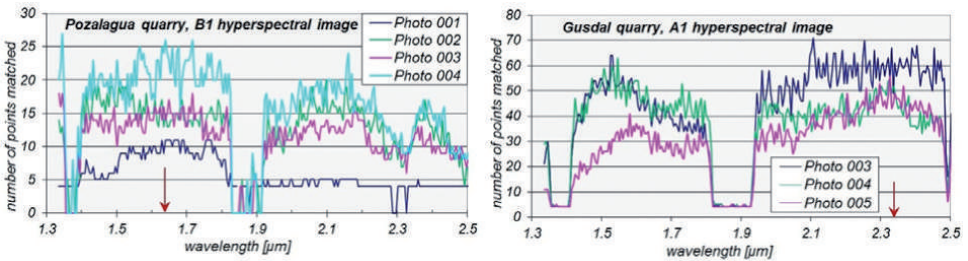


Fig. 3: Number of points matched between bands of the hyperspectral image and the overlapping photos. The wavelengths selected for matching are marked by red arrows.

as many interest points as possible, the SIFT detector was configured with values of 0 for the peak threshold, so that even points with the lowest contrast were detected, and 10 for the edge response threshold to filter weak edge responses. To reject matches that were too ambiguous, the VLFeat library uses a nearest neighbour algorithm with a distance ratio threshold, as suggested in LOWE (1999).

Due to many incorrect matches identified during a visual quality check, a homography model was fitted to the matched points using RANSAC. A homography model was used

(instead of a fundamental matrix), due to a very short baseline between matched images, and the fact that after pre-processing (section 4.2) the Nikon images were very close to a rotated, scaled, or warped version of the hyperspectral imagery. It is worth stressing that this model was only used for false match elimination and not utilized in any of the further orientation steps.

The number of homologous points found at each stage of the processing workflow is summarized in Tab. 1. Only overlapping image areas were taken into account in detec-

Tab. 1: Number of homologous points at different processing stages (SIFT = scale invariant feature transform).

HySpex image	SIFT points	Photo (pre-processed)	detected SIFT points		Matched points				RANSAC inliers			
					per photo	total	% per photo	% total	per photo	total	% per photo	% of total matches
B1	1490	Photo 001	375	1528	62	274	16.5	18	15	110	24.2	40
		Photo 002	337		68		20.2		24		35.3	
		Photo 003	370		71		19.2		31		43.7	
		Photo 004	446		73		16.4		40		54.8	
B2	1662	Photo 005	467	1727	64	253	13.7	15	7	66	10.9	26
		Photo 006	459		57		12.4		14		24.6	
		Photo 007	381		70		18.4		26		37.1	
		Photo 008	420		62		14.8		19		30.6	
A1	1581	Photo 003	441	1231	105	303	23.8	24	61	165	24.2	54
		Photo 004	396		104		26.3		53		35.3	
		Photo 005	394		94		23.9		51		43.7	

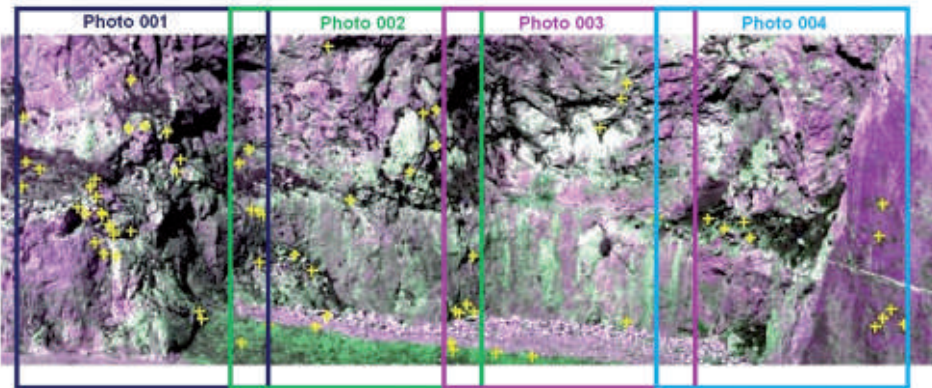


Fig. 4: Correctly matched points between B1 HySpex image (false colour composite shown here) and the overlapping Nikon photos.

tion of the SIFT interest points presented in Tab. 1. Due to the fact that the Nikon photos were acquired with 10 % side overlap (see Fig. 4) the total number of points found on the hyperspectral image and on the conventional photos are not directly comparable. The rate of points preliminarily matched in comparison to the number of SIFT keypoints detected is at the level of 12 %–26 % (column *Matched points* in Tab. 1). Taking into account the dissimilar spectral appearances of the two types of matched images, these values are satisfying and confirm the robustness of the scale invariant feature transform to image radiometric differences. The number of homologous points indicated by RANSAC as inliers was used to assess the matching accuracy (last column in Tab. 1), that is, a percentage of the correct matches in comparison to the total number of points matched. The estimated matching accuracy (26 %–54 %) is much lower than results reported in the case of matching images acquired at identical wavelengths (50 %–85 %, LOWE 2004). Nevertheless, the correct homologous point pairs could be reliably identified with the support of RANSAC and used in the later stages of the processing workflow.

4.4 Point Cloud Back-Projection

By themselves, the image coordinates of the homologous points in the hyperspectral imagery and the photos are not sufficient for the registration process. 3D object coordinates (X , Y , Z) are required, which may be derived indirectly from the lidar point cloud. In order to achieve that task, two processing steps were carried out for all conventional photos. Firstly, the point cloud was back-projected onto each photo plane using the collinearity condition, so that the relationship between each photo pixel and the object coordinates (X , Y , Z) was determined. This stage used the known projection centre, and the interior and exterior orientations from the pre-registered Nikon camera data. The effect of the photo downsampling algorithm was taken into account when defining the back-projection, in order to keep the correspondence between pixel and object point coordinates. In the second step, the exact object coordinates (sub-pixel) of each matched point

were interpolated in the back-projected point cloud image pixel array.

4.5 Spatial Resection

The orientation parameters of each HySpex image were established by a spatial resection (LUHMANN et al. 2007) using the geometric model for rotational linear-array panoramic cameras. The image and object coordinates of the control points, established automatically in previous processing steps, and the interior camera calibration parameters were supplied as input to the software Bundle (SCHNEIDER & MAAS 2007).

5 Results and Discussion

For the Pozalagua dataset, 110 control points were successfully matched using the SIFT interest operator between the 4 overlapping conventional photos and the HySpex B1 image (Fig. 4). 66 points were matched for the B2 image. The matching accuracy rates were estimated as 40 % for image B1 and 26 % for image B2. For the Gusdal A1 image, 165 homologous points were correctly matched with the three overlapping photos. In this dataset the matching accuracy was 54 %.

The values expressing matching accuracies (Tab. 1) are not directly comparable between datasets acquired in the two different locations. Not only were the image scales different (different imaging range, camera lens), but also the imaged geology was of a different mineral composition. The number of correctly found homologous points depends on the content/texture of the matched images, and thus on the both the 3D roughness and the 2D heterogeneity of the imaged surface. However, in the case of matching images acquired at different spectral ranges, the resulting number of points matched seems to be also material dependent. The difference in visual appearance between the materials in image A1 (Gusdal) and the conventional photos is much smaller than in the case of images B1 and B2 (Pozalagua). This can explain the relatively high (54 %) matching accuracy result for the A1 image. On the other hand, images B1 and

B2 contain very similar rock types, as they show the same outcrop wall, though a relatively large area of image B1 contains a freshly cut rock face that has a very distinctive texture pattern, and hence a higher matching accuracy (40%). Other factors, such as the amount of surfacing weathering and the infrared lighting conditions at the time of exposure, and therefore the signal strength, may also influence the number of extracted interest points.

The identified homologous points were successfully used in a spatial resection (RMS of planimetric coordinates of ground points be-

low 0.8 pix) to retrieve orientation parameters of the HySpex SWIR-320m scenes in the lidar project coordinate system. This in turn enabled the possibility to texture the lidar mesh model (BUCKLEY et al. 2010) with the HySpex processing products. An example of an outcrop model textured with both conventional photographs and results of hyperspectral classification (hyperspectral map) is shown in Fig. 5.

The hyperspectral image orientation parameters established using the processing workflow presented above have been used in

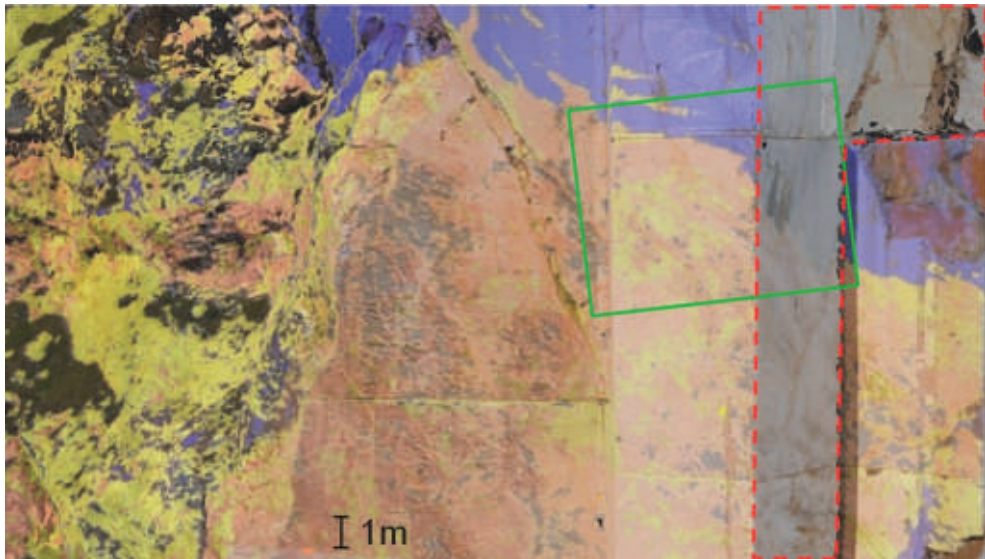


Fig. 5: 3D model textured with conventional photos (area outlined in red) and the results of hyperspectral image classification, where blue colours represent limestone and pink dolomite. Green rectangle marks the model sample shown in Fig. 6, right.

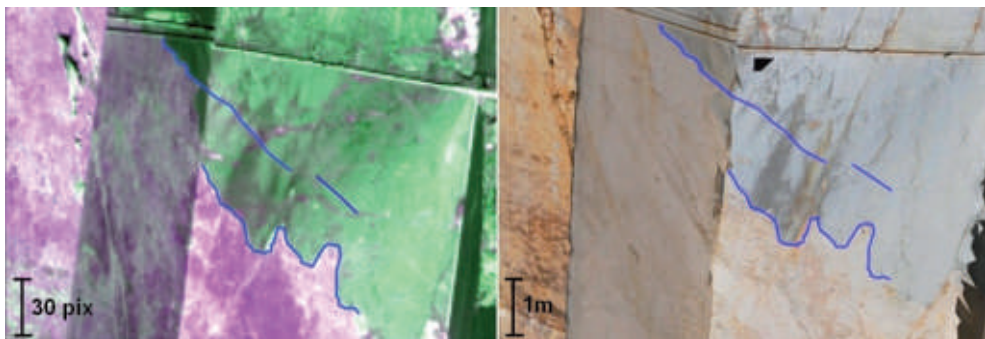


Fig. 6: 2D vectors digitized manually on a false colour RGB composite of the B1 HySpex image (left), and the corresponding 3D vectors displayed on the photorealistic model (right). Larger model overview shown in Fig. 5.

a visual quality check. Several clearly distinguishable features were digitized manually in the hyperspectral B1 image (Fig. 6, left). The collinearity condition with additional parameters (SCHNEIDER & MAAS 2006) was applied to the 2D pixel coordinates of each point of the digitized vector line on the hyperspectral image, using the newly established image orientation parameters. For each point, a ray was intersected with the lidar mesh to obtain a 3D point in the project coordinate space. The resulting 3D vectors were displayed together with the photorealistic outcrop model (Fig. 6, right). The correct position of the 3D vectors on the photorealistic model shows that HySpex image orientation parameters obtained using the proposed method can be used in the data integration process.

6 Conclusions and Future Work

In this paper a semi-automated method for integrating panoramic hyperspectral imagery into photorealistic outcrop models was presented. The automation level was increased by automatic point matching between the hyperspectral images and conventional photos. The SIFT interest operator proved to be robust to very different “radiometric conditions”, and capable of finding homologous points on images acquired in significantly different spectral ranges, i.e. in visible light (Nikon photos) and the short wave infrared spectrum (HySpex SWIR-320m imagery). The resulting matching accuracy rates are low when compared to the results obtained between data collected in similar spectral ranges; however, the elimination of false matches using RANSAC yields enough correct points to register the hyperspectral panoramic images to the lidar project coordinate system.

Although the control point distribution was not optimized for photogrammetric processing, the resulting HySpex image orientation enables the possibility to complement lidar outcrop models with spectral products, and is therefore a valuable technique for the domain end-users, geologists.

More work is required in order to evaluate the geometric accuracy of the determined orientation parameters. The quality of the devel-

oped data registration procedure can be further improved by using a bundle block adjustment to simultaneously orientate multiple images, instead of the single image spatial resection applied here. Application of a bundle block adjustment would be beneficial to check the stability of the interior orientation parameters of the HySpex SWIR-320m camera. In this case, matching should be restricted to areas of high data overlap, to reduce processing time. The control point distribution should be controlled and optimized for the purposes of photogrammetric applications. Influence of contrast enhancement on the final number of correct control points found will be investigated in order to force successful matches in low texture image areas.

Acknowledgements

This research is supported by the Research Council of Norway and FORCE (project number 193059). Statoil ASA and Sibelco Nordic are acknowledged for supporting the data collection. Norsk Elektro Optikk AS and Riegl GmbH are thanked for providing hardware and software support.

References

- BELLIAN, J.A., KERANS, C. & JENNETTE, D.C., 2005: Digital Outcrop Models: Applications of Terrestrial Scanning Lidar Technology in Stratigraphic Modeling. – *Journal of Sedimentary Research* **75** (2): 166–176.
- BÖHM, J. & BECKER, S., 2007: Automatic Marker-Free Registration of Terrestrial Laser Scans Using Reflectance Features. – *The International Archives of the Photogrammetry, Remote Sensing and Spatial Information Sciences XXXVI* (5/W17): 338–344.
- BUCKLEY, S.J., ENGE, H., CARLSSON, C. & HOWELL, J.A., 2010: Terrestrial Laser Scanning for Use in Virtual Outcrop Geology. – *The Photogrammetric Record* **25** (131): 225–239.
- BUCKLEY, S.J., HOWELL, J.A., ENGE, H.D. & KURZ, T.H., 2008: Terrestrial Laser Scanning in Geology: Data Acquisition, Processing and Accuracy Considerations. – *Journal of the Geological Society* **165** (3): 625–638.
- CLARK, R.N. & ROUSH, T.L., 1984: Reflectance Spectroscopy: Quantitative Analysis Techniques

- for Remote Sensing Applications. – *Journal of Geophysical Research* **89** (B7): 6329–6340.
- CLARK, R.N., KING, T.V.V., KLEJWA, M., SWAYZE, G.A. & VERGO, N., 1990: High Spectral Resolution Reflectance Spectroscopy of Minerals. – *Journal of Geophysical Research* **95** (B8): 12653–12680.
- DURDA, F., 2012: NTSC Primer. http://nemesis.lonestar.org/reference/internet/web/color/ntsc_primer.html (February 2012).
- FISCHLER, M.A. & BOLLES, R.C., 1981: Random Sample Consensus: a Paradigm for Model Fitting with Applications to Image Analysis and Automated Cartography. – *Graphics and Image Processing* **24** (6): 381–395.
- FORKUO, E.K. & KING, B., 2004: Automatic Fusion of Photogrammetric Imagery and Laser Scanner Point Clouds. – *The International Archives of the Photogrammetry, Remote Sensing and Spatial Information Sciences* **XXXV** (B4): 921–926.
- FÖRSTNER, W., 1986: A Feature Based Correspondence Algorithm for Image Matching. – *The International Archives of the Photogrammetry, Remote Sensing and Spatial Information Sciences* **XXVI** (3/3): 150–166.
- GONZÁLEZ-AGUILERA, D., RODRÍGUEZ-GONZÁLEZ, P. & GÓMEZ-LAHOZ, J., 2009: An Automatic Procedure for Co-Registration of Terrestrial Laser Scanners and Digital Cameras. – *ISPRS Journal of Photogrammetry and Remote Sensing* **64**: 308–316.
- HARRIS, C. & STEPHENS, M., 1988: A Combined Corner and Edge Detector. – *4th Alvey Vision Conference*: 147–151, Alvey, UK.
- JAZAYERI, I. & FRASER, C.S., 2010: Interest Operators for Feature-Based Matching in Close Range Photogrammetry. – *The Photogrammetric Record* **25** (129): 24–41.
- KURZ, T.H., BUCKLEY, S.J., HOWELL, J.A. & SCHNEIDER, D., 2011: Integration of Panoramic Hyperspectral Imaging with Terrestrial Lidar Data. – *The Photogrammetric Record* **26** (134): 212–228.
- KURZ, T.H., DEWIT, J., BUCKLEY, S.J., THURMOND, J.B., HUNT, D.W. & SWENNEN, R., 2012: Hyperspectral Image Analysis of Different Carbonate Lithologies (Limestone, Karst and Hydrothermal Dolomites): the Pozalagua Quarry Case Study (Cantabria, North-west Spain). – *Sedimentology* **59** (2): 623–645.
- LINGUA, A., MARENCHINO, D. & NEX, F., 2009: Performance Analysis of the SIFT Operator for Automatic Feature Extraction and Matching in Photogrammetric Applications. – *10th CESC Conference* **9** (5): 3745–3766.
- LOURENÇO, M., BARRETO, J.P. & MALTI, A., 2010: Feature Detection and Matching in Images with Radial Distortion. – *ICRA'2010*: 1028–1034.
- LOWE, D., 1999: Object Recognition from Local Scale-Invariant Features. – *7th IEEE International Conference on Computer Vision* **2**: 1150–1157.
- LOWE, D., 2004: Distinctive Image Features from Scale-Invariant Keypoints. – *International Journal of Computer Vision* **60** (2): 91–110.
- LUHMANN, T., ROBSON, S., KYLE, S. & HARLEY, I., 2007: Close range photogrammetry: principles, techniques and applications. – 528 pp, Wiley, UK.
- NEVILLE, R.A., LIXIN, S. & STAENZ, K., 2004: Detection of Keystone in Imaging Spectrometer Data. – *SPIE, April 2004*: 208–217, Orlando, FL, USA.
- NIETO, J.I., MONTEIRO, S.T. & VIEJO, D., 2010: 3D Geological Modelling Using Laser and Hyperspectral Data. – *IGARSS 2010 Symposium*: 4568–4571.
- OSTIAK, P., 2006: Implementation of HDR Panorama Stitching Algorithm. – *10th CESC Conference* **2006**: Castá-Papiernicka.
- PICARD, D., CORD, M. & VALLE, E., 2009: Study of SIFT Descriptors for Image Matching Based Localization in Urban Street View Context. – *CMRT2009 Conference*, Paris.
- RIEGL LMS-Z420i, Brochure, http://www.riegl.com/uploads/tx_pxpriegldownloads/10_Data_Sheet_Z420i_03-05-2010.pdf (February 2012).
- SCHNEIDER, D. & MAAS, H.-G., 2006: A Geometric Model for Linear-Array-Based Terrestrial Panoramic Cameras. – *The Photogrammetric Record* **21** (115): 198–210.
- SCHNEIDER, D. & MAAS, H.-G., 2007: Integrated Bundle Adjustment with Variance Component Estimation – Fusion of Terrestrial Laser Scanner Data, Panoramic and Central Perspective Image Data. – *The International Archives of the Photogrammetry, Remote Sensing and Spatial Information Sciences* **XXXVI**: 373–378.
- VAN DER MEER, F.D., 2004: Analysis of Spectral Absorption Features in Hyperspectral Imagery. – *International Journal of Applied Earth Observation and Geoinformation* **5** (1): 55–68.
- VEDALDI, A. & FULKERSON, B., 2008: {VLFeat}: An Open and Portable Library of Computer Vision Algorithms, <http://www.vlfeat.org> (February 2012).

Addresses of the Authors:

ALEKSANDRA A. SIMA, SIMON J. BUCKLEY & TOBIAS H. KURZ, Centre for Integrated Petroleum Research (Uni CIPR), Postboks 7810, 5020 Bergen, Norway, Tel.: +47-555-83-670, -458, -646, e-mail: {aleksandra.sima}{simon.buckley}{tobias.kurz}@uni.no

DANILO SCHNEIDER, Technische Universität Dresden, Germany, Tel.: +49-351-463-33144, e-mail: danilo.schneider@tu-dresden.de

Manuskript eingereicht: März 2012
Angenommen: Mai 2012